Development of Thermomechanical Processes as an Alternative to Grain Refiners in 18 Carat Gold Alloys

Mirko Pigato, Luca Pezzato, Claudio Cason, and Manuele Dabalà

The use of grain refiners, such as iridium, in 18 kt gold alloys is a common practice in jewelry industrial applications. The use of these elements leads, however, to an increase in the costs of raw materials and greater attention during the solidification phases and during the refining and recycling of alloys is required. This work aims to demonstrate that through the optimization of thermo-mechanical processes, it is possible to obtain a result comparable to that obtained with refiner in terms of workability, mechanical and aesthetic properties and corrosion behavior. The study focused on evaluating the grain growth in annealing processes after plastic deformation, also examining the casting phase and the effect of the different cooling rates. The samples, after the different thermo-mechanical treatments, were characterized in terms of microstructure, grain size and micro-hardness comparing the results with the ones of an iridium-containing alloy. The results showed that with proper optimization of annealing time is possible to obtain, without grain refiners, gold alloys with properties similar to ones obtained with Iridium as a grain refiner.

1. Introduction

The use of grain refiners in gold alloys in the production of items by cold deformation and casting processes is nowadays a common practice in jewelry industries (Ref 1, 2). These elements can act in the solidification and recrystallization phases. Considering the solidification stage: rare earth (yttrium), boron, barium and calcium have been studied; they stimulate heterogeneous nucleation through the dispersion of fine oxide particles thanks to their marked reactivity with oxygen and their low solubility in gold alloy (Ref 3). In the case of zirconium + boron and cobalt + boron, their effect is probably associated with the formation of intermetallic compounds. Small quantities of iridium and ruthenium, characterized by high melting temperatures and low solubility in gold alloys, are more often employed. They guarantee a reduction in the crystalline grain, favoring the formation of nucleation centers during cooling and increasing the stability of small radius solidification cores (Ref 4). All the elements mentioned above can act also in the recrystallization stage, thanks to their tendency to segregate and precipitate at the grain boundary, slowing down the grain growth during annealing (Ref 5). This thermal treatment is typically employed in the jewelry industry because is an essential step to recover ductility in processes where cold deformation is foreseen, to obtain a more uniform structure and to control the grain size during recrystallization.

Another widely used element particularly effective in reducing crystals growth in this phase is cobalt (Ref 4). However, grain refiners are commonly very expensive, and incorrect employment can create a series of side effects. For example, their tendency to segregate or to form oxides causes embrittlement of the material or creates hard spots that make the polishing very complicated (Ref 6). A lot of studies are present in literature regarding the control of grain growth in jewelry industries. In particular, they focus or on the use of grain refiners (Ref 2, 4, 5) or on optimizing a thermo-mechanical process (Ref 7, 8), but no works regarding the comparison and evaluation of the two methods of grain refining on the same alloy can be found. This work aims to analyze how the use of refiners, iridium in this case, can be replaced by thermo-mechanical processes through the optimization of the production process of hollow chains in 18kt gold alloy. The objective is the reduction in the costs of the raw material, obtaining a result comparable with the iridium-containing alloy, in terms of grain size, hardness, color and corrosion resistance. In detail in the present study, three 18 carat alloys (one with iridium and two without) were cast continuously in the form of foils, which are brought to a final thickness through three rolling steps, interspersed with two annealing steps. During the casting phase, the effect of two different degrees of subcooling was analyzed. Moreover, during the first heat treatment, the effect of different annealing times on the grain size and the hardness was tested, thus comparing the alloys without iridium to those with the refiner.

2. Materials and Method

2.1 Materials

An Iridium refined 18 carat gold alloy has been compared with 2 different not refined 18 kt gold alloy: a 4N standard and a not standard alloy. The composition range of the alloys can be found in Table 1.

Mirko Pigato, Luca Pezzato, and **Manuele Dabalà**, Department of Industrial Engineering, University of Padova, Via Marzolo 9, 35131 Padova, Italy; and **Claudio Cason**, Filk S.p.a, Via dell'Industria 8, 36065 Mussolente, Vicenza, Italy. Contact e-mails: mirko.pigato@unipd.it and mirko.pigato@gmail.com.

Table 1   Compositions of 18 carat alloys

18 kt Alloys	Au wt.%	Cu wt.%	Ag wt.%	Zn wt.%	Ir wt.%
Alloy 1	75	14.5–14.6	7.7–7,8	2.6–2,7	0.05
4N	75	16	9	–	–
Alloy 2	75	15.2–15.3	8.4–8.5	1.3–1.4	–
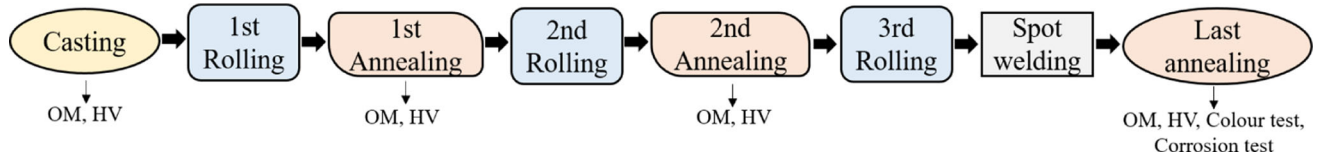
Figure 1   Schematic representation of the process and tests. OM (Optical Microscope), HV (Hardness Vickers)

Table 2   Parameters of the process

	Rollings		
	1ˢᵗ Rolling	**2ⁿᵈ Rolling**	**3ʳᵈ Rolling**
Initial thickness	5,7 mm	2,5 mm	0,85 mm
Final thickness	2,5 mm	0,85 mm	0,55 mm
Section reduction	50%	65%	35%
Annealings after rolling			
Annealing Temperature		**Annealing Time**	
660 °C		45 min	
Spot-welding			
Materials involved		**Electric current**	
Gold foil + iron foil		20000 A	
Annealing after spot welding			
Annealing Temperature		**Annealing Time**	
930 °C		2 min	
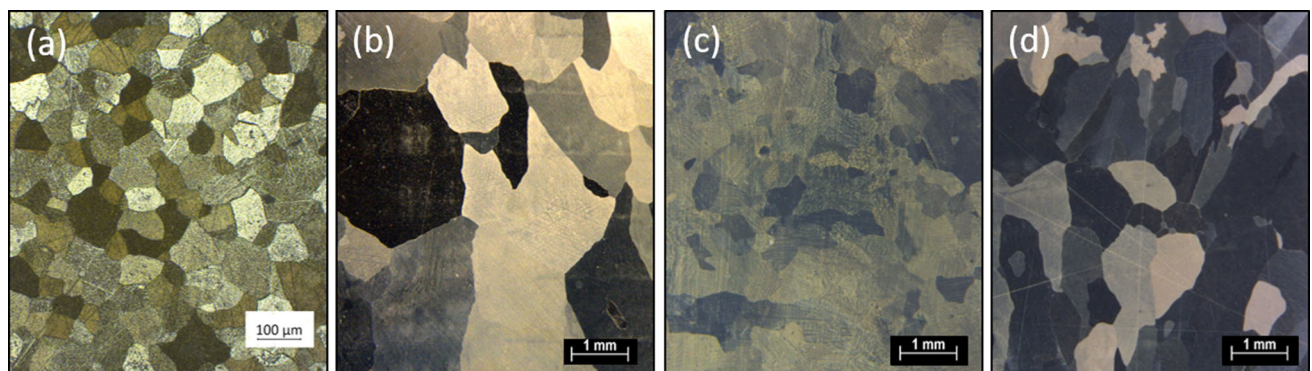
Figure 2   Microstructures of casting samples. Horizontal furnace: (a) Alloy 1, (b) Alloy 4N. Vertical furnace: (c) Alloy 4N, (d) Alloy 2

2.2 Experimental Procedure

The casting furnaces managed in the study are two induction furnaces one with a horizontal and the other with vertical output. Both the furnaces have a quenching system that immediately cools down the plate after solidification. The rolling mill used for thickness reductions has 5 pairs of adjustable cylinders, and it has been used for all thickness
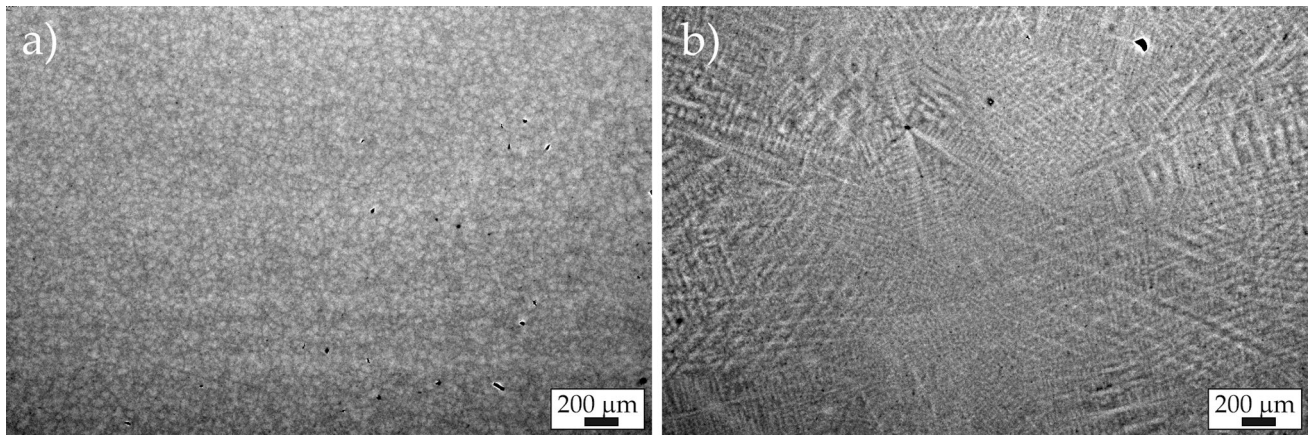
Figure 3 SEM images (backscattered electron mode) of (a) alloy 1 and (b) alloy 2 after casting
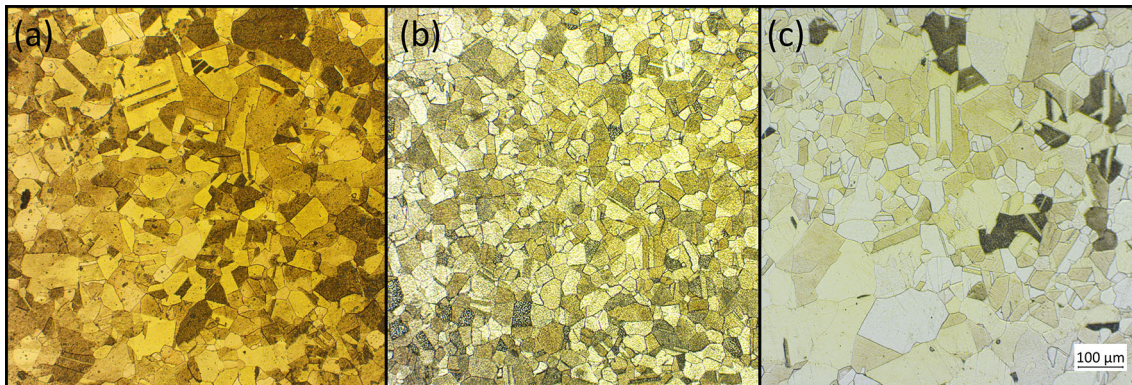

Figure 4 First annealing at 660°C for 40min after a section reduction of 50%. (a) 4N. (b) Alloy 1. (c) Alloy 2. Grains dimension: (a) 52± 4 μm. (b) 29 ±2 μm (c) 48 ± 3 μm

reductions. The annealing furnaces are resistance ovens where the treatments take place statically and the foils are quenched by immersion in water immediately after the thermal process. Annealing times tests were carried out in a batch oven by cutting from the foil a sample of 3 cm and annealing it with a skein of 5 kg of iron to simulate the thermal inertia of the load during production.

The sampling was carried out by cutting the sheets after each processing step, producing samples with a length of approximately 3 cm and a variable width depending on the step studied.

In order to analyze the microstructure of the samples, these were mounted in a phenolic resin, ground with abrasive papers (500, 800, 1200, 4000 grit) and polished with clothes and diamond suspensions (6 and 1 microns).

Once the sample was polished, the surface was etched by an electrochemical attack (20% HCl at 1.5V for 15-30 seconds, depends on samples). The optical microscope (OM) observation was performed by means of a LEICA DMRE microscope. The microhardness evaluation was carried out with a Vickers Leitz Wetzlar micro-hardness tester with a load of 300g. The grain size calculation was performed accordingly to ASTM E112-13 method. The macro-hardness was evaluated by means of Rockwell HRB hardness performed by AFFRI MRS 250 in according to ASTM E18-20.
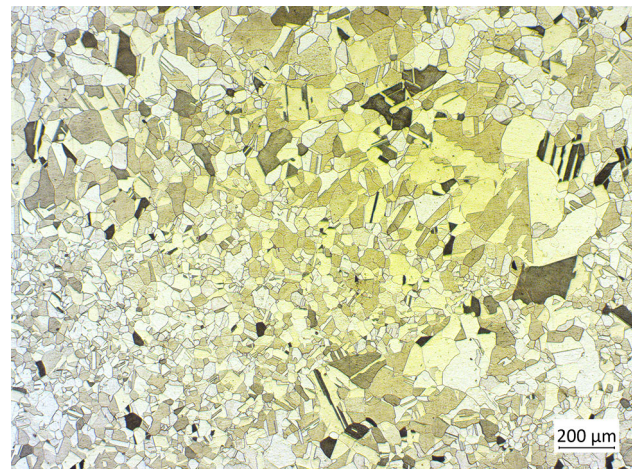

Figure 5 First annealing of alloy 2

Cambridge Stereoscan 440 scanning electron microscope equipped with a Philips PV9800 EDS was used to observe the presence segregation during casting, working in backscattered electron mode.
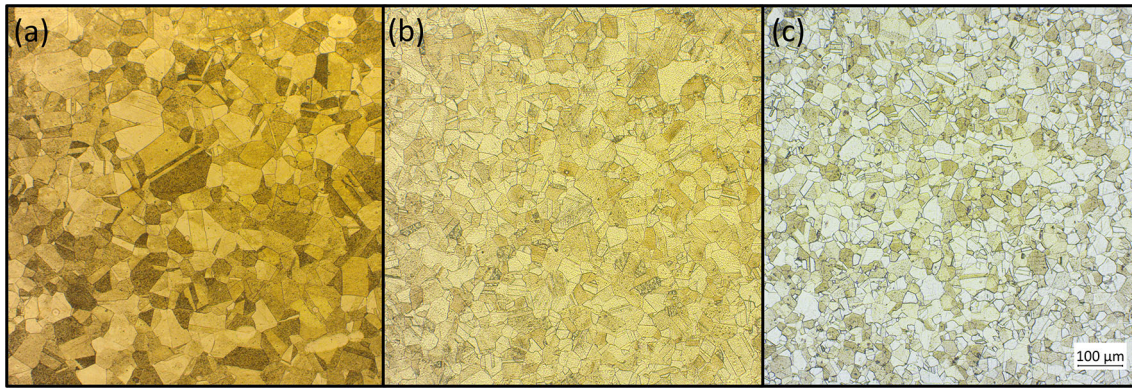
Figure 6 Second annealing at 660°C for 40min after a section reduction of 50%. (a) 4N. (b) Alloy 1. (c) Alloy 2 Grains dimension: (a) 46 ± 2 μm. (b) 30 ±1 μm. (c) 24 ± 3 μm
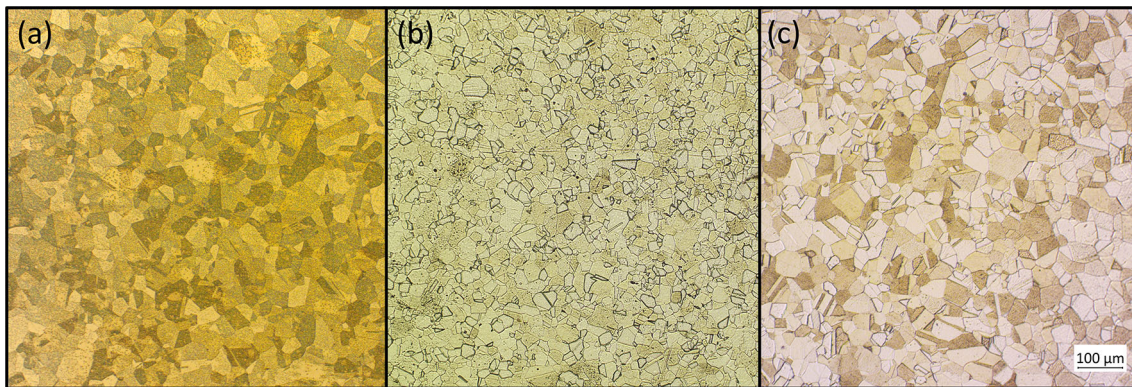

Figure 7 Annealing after spot welding at 930°C for 2min after plaiting (a) 4N. (b) Alloy 1. (c) Alloy2. Grains dimension: (a) 39± 2 μm. (b) 22 ± 1 μm (c) 31 ± 1 μm
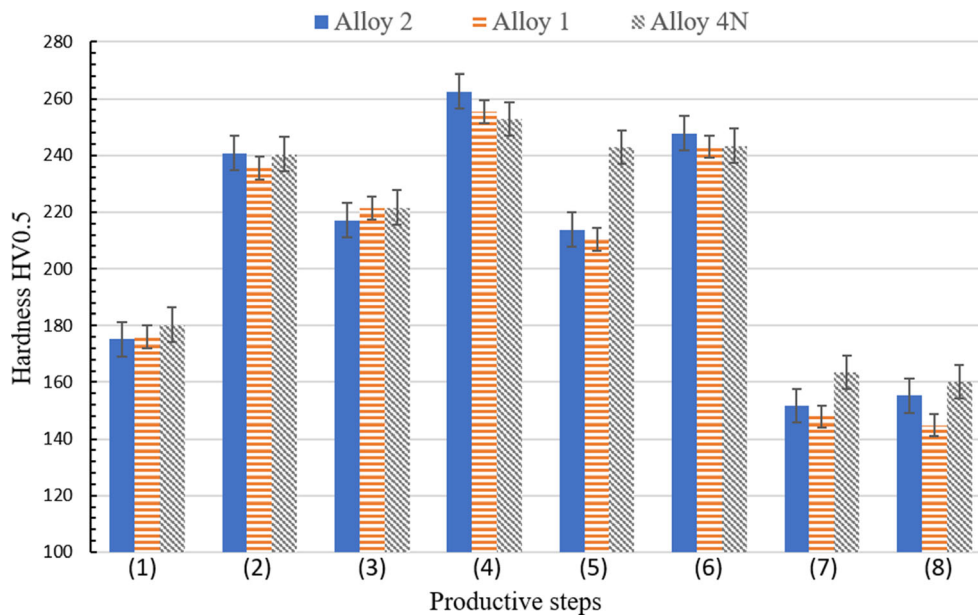

Figure 8 Hardness trend of the three alloys during every productive step (1) 1° Rolling, (2) 1° Annealing (3) 2° Rolling (4) 2° Annealing (5) 3° Rolling (2) Spot welding (2) Annealing after spot welding

The samples were analyzed by x-ray diffraction (XRD), with a Siemens D500 diffractometer, using a Cu-Ka radiation source nickel-filtered (k = 0.15405 nm) operating at 40 kV and 30 mA, in order to prove the presence of hardening phase.

To determine the color of the goldsmith's alloy, the CIElab coordinates were identified using a KONIKA MINOLTA CM 2600d-C spectrophotometer. Measurements were made with an illuminant D65 which represents the standard simulating the daylight, with a sample inclination of 10° in Specular Included mode.

The corrosion resistance was evaluated with potentiodynamic polarization tests in artificial perspiration (ISO 3160-2). Potentiodynamic polarization tests were performed with an AMEL 2549 Potentiostat, a platinum electrode as the counter electrode, with a scan rate of 8×10^{-4} Vs-1 and a saturated calomel electrode as the reference electrode (SCE). The measures were performed after 30 min of open circuit voltage (OCV) stabilization in the potential range -0.6 / 0.8 V. For each sample, three tests were performed to assure reproducibility.

The three curves for each sample are substantially the same, so only one is reported for clarity reasons.

2.3 Industrial Production Process Analyzed

In Figure 1 is reported a scheme of the industrial process, consisting of casting, cold deformation and annealing, that was studied in this work in order to obtain un-refined alloy with properties comparable to the one with iridium as grain refiner.

As mentioned above, the furnaces used to melt the alloys are a horizontal and a vertical output induction furnace. The foil coming out from the die is guided by rollers which regulate the discontinuous exit of the bar. Subsequently, the casting of raw material undergoes a thickness reduction. However, this process must take place gradually, alternating the deformation processes with annealing heat treatments, through which it will be possible to recover deformability and workability, lost during work hardening caused by cold deformation, and to recrystallize the material. The details of the production process with the different steps of cold working and annealing are
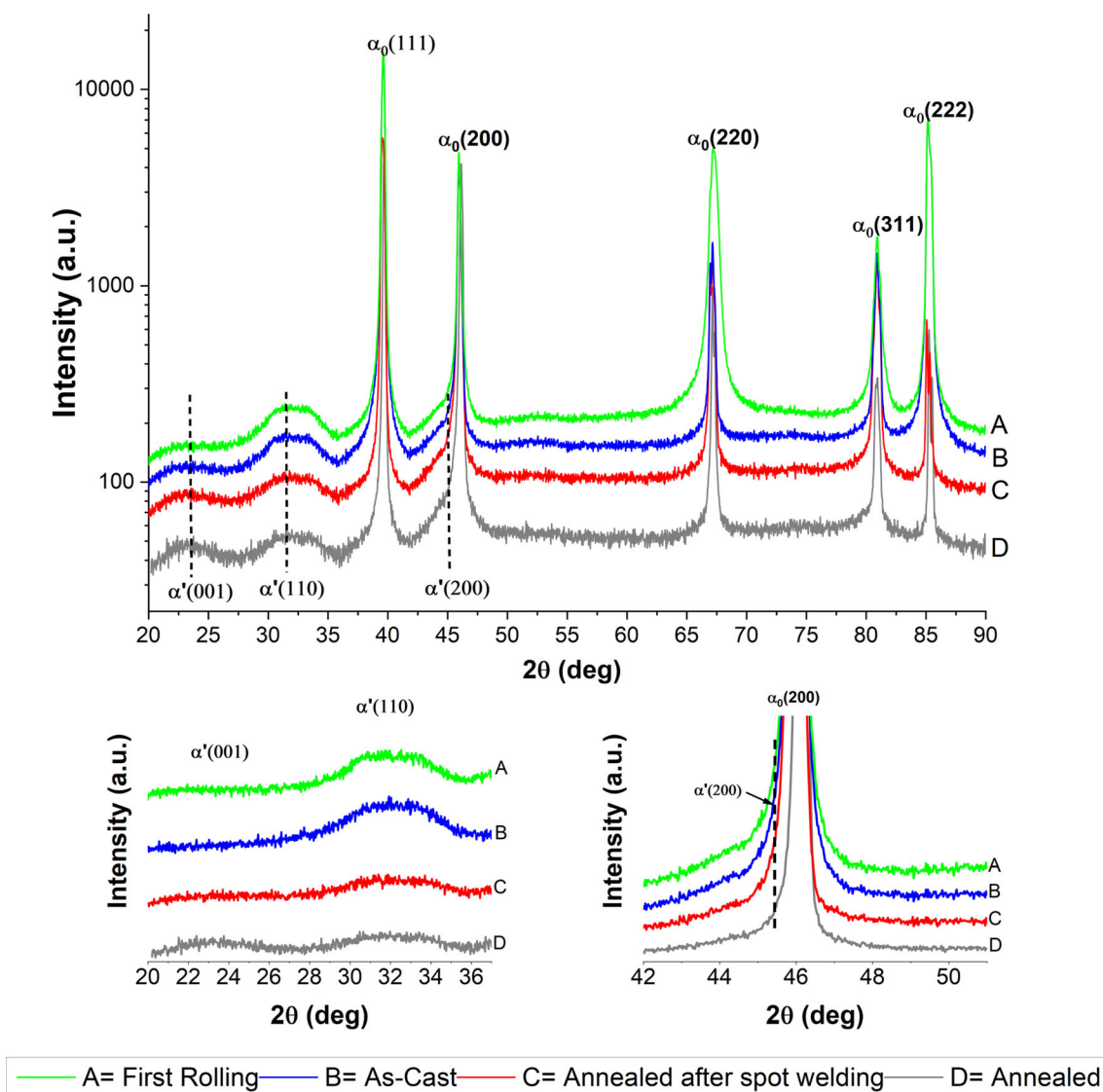

Figure 9 XRD analysis of alloy 2, A) after first rolling, B) As-Cast, C) Annealed after spot welding, D) after First annealing

summarized in Table 2. At the end of the steps described in Figure 1, the foil is coupled, trough spot welding process, to an iron foil that acts as a reinforcement core during subsequent deformations and is then eliminated by acid dissolution in order to produce empty chains. After the coupling, the foils are annealed in a continuous oven at 930 ° C for approximately 2 minutes. At the exit, the foil is immediately cooled with jets of water.

In this work, samples after each production process were characterized in terms of microstructure and hardness to evaluate the possibility to eliminate the grain refiner. Moreover, different annealing times, between 15 and 40 min for 4N alloy and alloy 2, were tested for the first annealing step in order to optimize the annealing. After this test, the samples were characterized in terms of microstructure and hardness.

3. Results and Discussion

3.1 Casting

The absence of Iridium in this phase is critical; using the same production parameters and the horizontal output furnace, the grains dimension increases significantly. The grains in 4N samples are bigger and stretched if compared to the refined one. Using the vertical output furnace, that has a more powerful cooling system (thanks to a longer cooling zone and a graphite's die more conducible), it is possible to observe a smaller dimension of the grains (Figure 2).

Table 3 CIELab coordinates of alloys studied and their distance (ΔE) from alloy 1

Alloy	L	a	b	ΔE (from Alloy1)
1	89.59	4.4	20.8	–
2	88.15	6.06	21.92	2.5
4N	88.46	7.58	21.56	3.5

During metal casting, the crucible base temperature in the horizontal and vertical furnaces was 910°C and the die temperatures were 700°C and 660°C, respectively. Vertical furnace permit to have a greater subcooling degree and permit to reduce considerably the dimension of the grains, but it is not enough to compensate the effect of the refiner that allows having a grain dimension of 60 μm (Standard deviation = σ = 2). This dimension agrees with the data reported by J.P. Nielsen et al. (Ref 4) on the effect of iridium as grain refiner. Moreover, the refining effect given by Iridium in our case is also comparable with the one observed in (Ref 9) where a reduction in more than 6 times in the size of the grain is observed with the use of 0.0055% of iridium in an 18 kt gold yellow alloy. There is not a notable difference between the structure of 4N alloy and alloy 2 regarding the grain size (Figure 2).

In Figure 3, segregations of Alloy 1 and Alloy 2 are analyzed at SEM and compared. As can be observed, well developed dendritic structure characterized Alloy 2, whereas Alloy 1 appears to possess more equiassic microstructure. Semi-quantitative EDS analysis evidence that in both case Ag and Cu segregate and enrich liquid during solidification, in fact, zones rich in these elements can be found or at the grain boundaries or between the secondary dendritic arms. Other studies show different segregation phenomena of Cu and Ag during casting in a graphite crucible (Ref 10), probably induced by the different casting system.

3.2 Annealing and Recrystallization

The refined alloy starts to recrystallize from a fine structure; furthermore, iridium reduces the growth rate of new grains by slowing down the diffusion at their boundary. Pezzato et al. (Ref 7) observed that starting from an as-cast 5N gold alloy refined with iridium with a grain size of 60 μm it is possible to obtain after two steps of deformation and annealing a grain dimension of 20 μm. Considering the difference in the annealing time, the results are comparable with what observed in this study. During the first annealing, alloys without refiners reduce drastically their initial grain dimension (Figure 4), but they do not achieve a good homogeneity in crystals size as can be see in Figure 5. A wide distribution of the grain
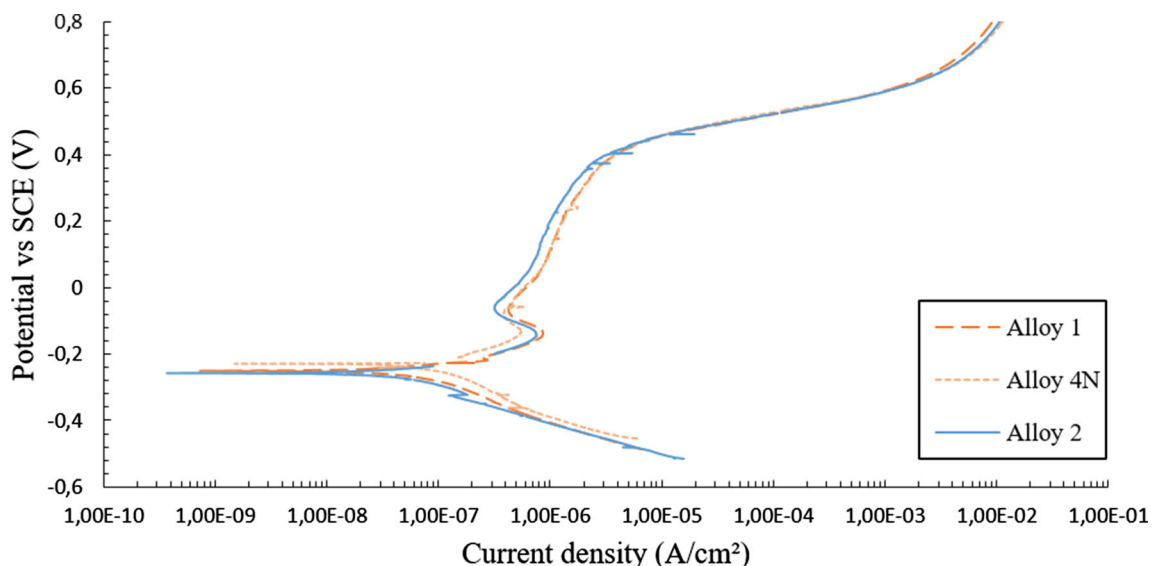
Figure 10 Potentio-dynamic curves in artificial perspiration of the three alloys after last step studied (annealing after spot welding)

dimension can be in fact observed. During deformation, initial grains of large dimensions react differently according to their crystallographic orientation and therefore behave differently also in annealing treatment, causing ununiform recrystallization. (Ref 11)

Second annealing at 660°C for 40 minutes is done after a second section reduction of 65%. In this operation, all the microstructures are more uniform, probably due to reduced initial crystal size, and the grain dimension of Alloy 2 is lower than alloy 1. (Figure 6)

Table 4 Corrosion potential and current density of the three alloys

Alloy	Corrosion potential, V	Corrosion current density, A/cm^2
1	− 0,25	8 E-08
4N	− 0,23	9 E-08
2	− 0,26	7 E-08

3.3 Annealing After Spot-Welding

After the last rolling deformation and the spot-welding process, the plate is characterized by a partial recrystallized structure and the foil needs to be annealed in a continuous oven at 930 ° C for 2 minutes. As can be seen in Figure 7, the annealing process allows the products to homogenize their structure and complete recrystallization. Alloy 1 has the smaller average grain size, probably due to the capacity of iridium to control the grain grow during recrystallization. Alloy 2 has finer structure respect to 4N alloy, as observed also in the previous thermal treatment.

3.4 Hardness Evolution

The hardness is used as strain hardening index, its trend shows the same behavior for alloys 1 and 2, and a sufficient stress relief occurs after every deformation (Figure 8). During annealing, the ductility necessary for the next rolling steps is recovered. The minimum hardness is reached after the plating and the annealing of the plated, to ensure good workability during subsequent processing. 4N alloy follows the common trend of other two alloys except for the second annealing. In thermal treatments of 18 Kt gold alloys or any process where the material cools down from a temperature where the completely disordered phase is stable, rapid cooling is necessary to reduce at minimum the precipitation of hardening
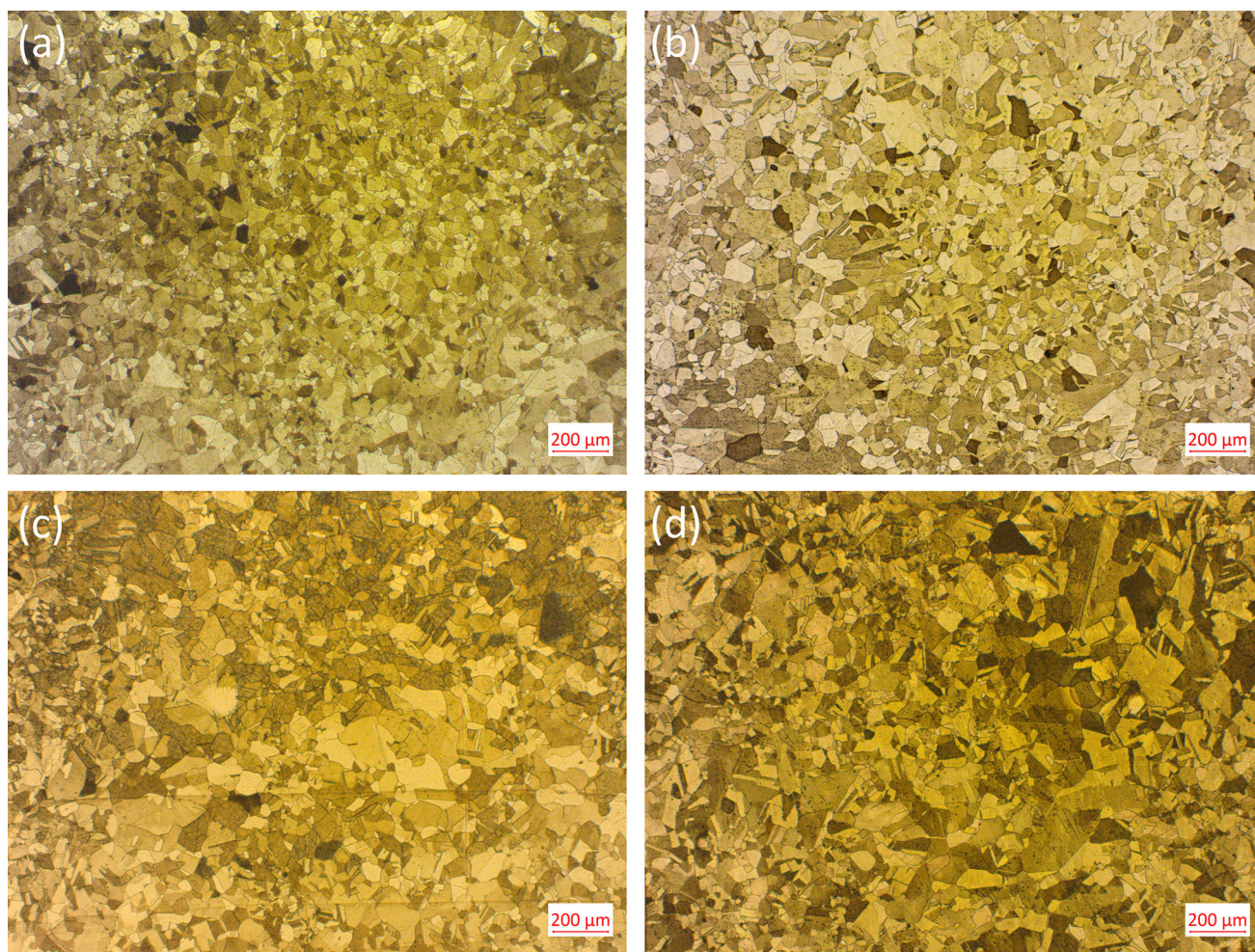

Figure 11 First annealing tests of alloy 4N. Annealing time (a) 15, (b) 20, (c) 30, (d) 40 minutes at 660°C
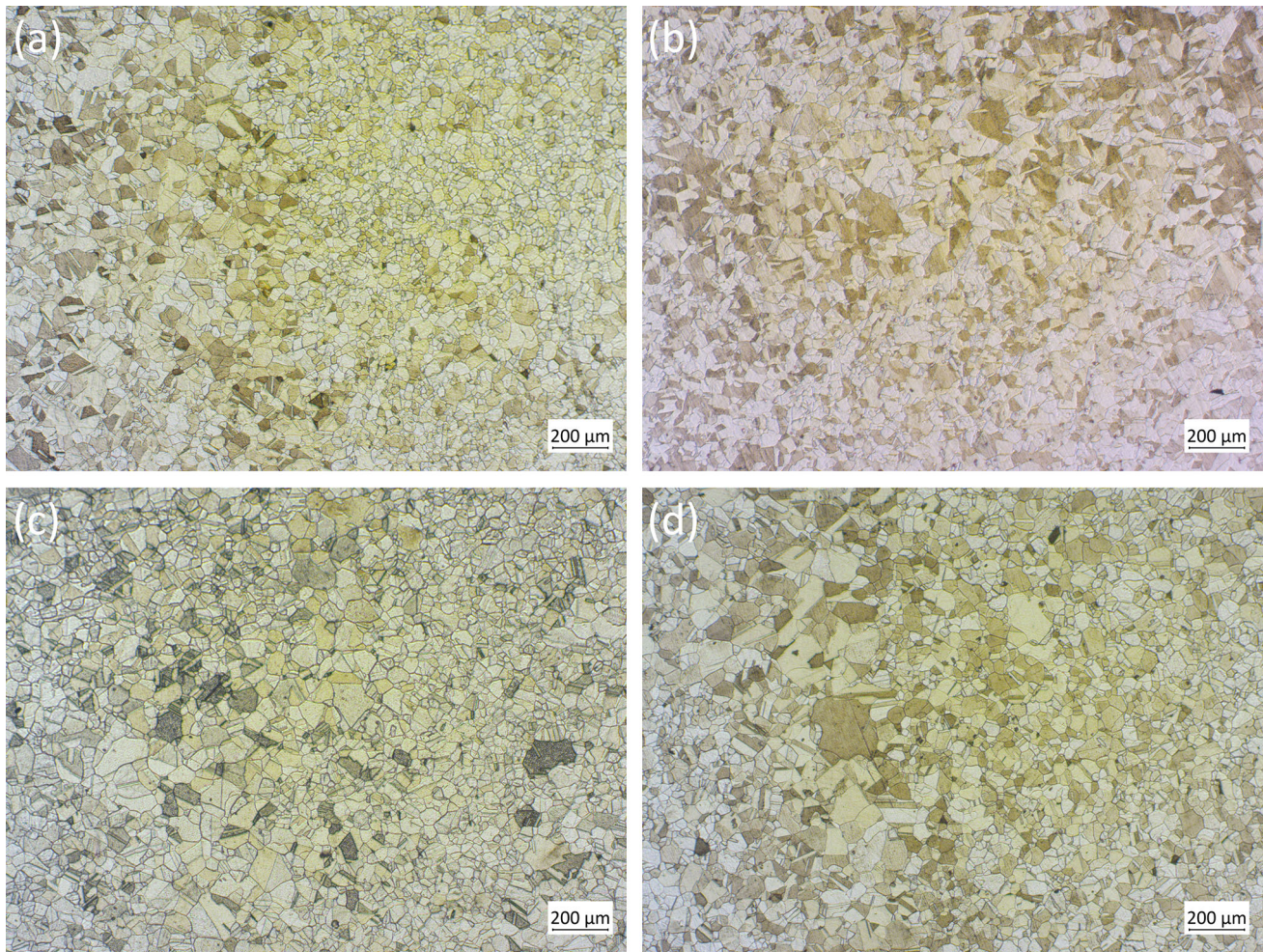
Figure 12 First annealing tests of alloy 2. Annealing time (a) 15, (b) 20, (c) 30, (d) 40 minutes at 660°C

phases such as AuCuI or AuCuII. XRD analysis, reported in Figure 9, confirms in our case the presence of ordered phases AuCuI (α'). Garcia-Gonzalez et al. observed in (Ref 12) that the microstructure of an 18 kt red gold alloy after quenching in water from 660°C is characterized by a metastable disordered FCC matrix (α_0), a nanometer-size dispersion of coherent and chemically ordered domains (α') within the disordered phase and minor Ag-rich phases. The authors conclude that the nature of phase transformations and their kinetics depend on cooling rate.

All the alloys studied in this work show the same behavior during the production process, and in Figure 9 patterns of Alloy 2 are presented as an example to understand the evolution of phases during the process. Disordered phase's diffraction peaks of as-cast and rolled samples evidence a textured microstructure. $\alpha'(110)$ peak remains unchanged during the first rolling step, in fact, 50% reduction in thickness does not destroy the ordered structure in accordance with (Ref 12). In the annealed and annealed after spot welding samples, the intensity of $\alpha'(110)$ decreases, whereas the $\alpha'(001)$ increases, probably due to the change in texture.

It is not possible to exclude the presence of long-range antiphase domain (AuCuII) in the patterns in Figure 9. In fact,

in (Ref 13) for a composition analogous to the alloys examined in this study it is possible to observe the formation of AuCuII depending on the ageing temperature.

3.5 Color Analysis

Results collected in Table 3 show a considerable chromatic difference between the 4N alloy and Alloy 1. 4N is an alloy which is also called "rose gold" and is the standard to define this type of coloring. A smaller quantity of copper allows to obtain a less reddish color; moreover, the absence of zinc does not allow to buffer the effect of copper by increasing the factor "a" in the coordinates of the CIELab space (Ref 14). Overall, 4N has a more saturated color and an $\Delta E = 3.5$, which means that even a non-expert observer can distinguish the two colors. The distance between the colorimetric coordinates of Alloy 1 and 2 is still perceptible but commercially acceptable ($\Delta E < 3$ (Ref 15)). A more similar composition and the presence of zinc permit to have a comparable color.

3.6 Corrosion Resistance

The corrosion resistance of the 18 kt gold alloys was tested after the last step studied (annealing after spot welding), where

a good homogenized structure is reached in all the samples. Observing the almost complete overlap of the curves in Figure 10, it is clear that the different alloys have the same corrosion behavior in artificial perspiration. Also, from the quantitative point of view the corrosion potentials and corrosion current densities graphically extrapolated (Table 4) are the same for all the alloys. Results prove that the residual stresses and the homogeneity of the three alloys are similar, according to (Ref 16). This result evidences that the absence of iridium does not cause problems regarding corrosion resistance. The results are also in accordance with what observed by Rainer Süss et al. (Ref 17) that prove that the use of different grain refiners does not compromise the corrosion resistance of 18 ct yellow gold alloy, in terms of weight loss in artificial perspiration for 7 weeks.

3.7 1st Annealing Optimization

To optimize the annealing process, in particular the first one, and obtain a smaller grain size, different annealing times were tested for not refined alloys (4N and Alloy 2), and the results compared to Alloy 1. Tests were carried out at 40, 30, 20 and 15 minutes at 660 ° C with subsequent quenching in water.

In Figure 11 for 4N alloy and in Figure 12 for Alloy 2, it can be observed that, in both cases, the recrystallization process is completed already after 15 minutes of treatment. As expected, over time the average grain size increases and the smaller grains disappear with a consequent increase in the larger ones, always maintaining a considerable degree of inhomogeneity.

In Figure 13 is reported the evolution of the grain size with the annealing time of Alloy 2 and 4N, comparing it with the corresponding value of Alloy 1 (highlighted with a horizontal line). For Alloy 4N, it is possible to obtain a grain dimension similar to the refined reference only with an annealing time under 15 minutes (provided that, at shorter times, the recrystallization is complete). For all annealing times, the grain size

of Alloy 2 in these tests is smaller than that observed with the 4N alloy. The reduction is slight but permits to have a result equal to the Alloy 1 with a treatment time between 15 and 20 min.

The hardness data, reported in Table 5, show that this parameter is independent from the annealing time. It can be stated that the stress condition of the material is identical for all annealing times and that therefore the recovery of ductility and workability is the same. At this temperature, recovery occurs before 15 minutes of treatment and, in this time-laps, the increase in grain size does not affect the hardness.

The data obtained from the annealing test can be analyzed through the Burke and Turnbull analysis (Ref 18) of grain growth kinetics, which utilized a power law to link the grain size with the permanence time at a certain temperature (Eq. 1).

$$d^n - d_o^n = Kt \qquad \text{(Eq 1)}$$

In the equation, d is the average grain dimension at the time t, d_o is the initial grain size, K is a constant depending on the

Table 5 Hardness of first annealing samples of alloy 4N and Alloy 2 (HRB)

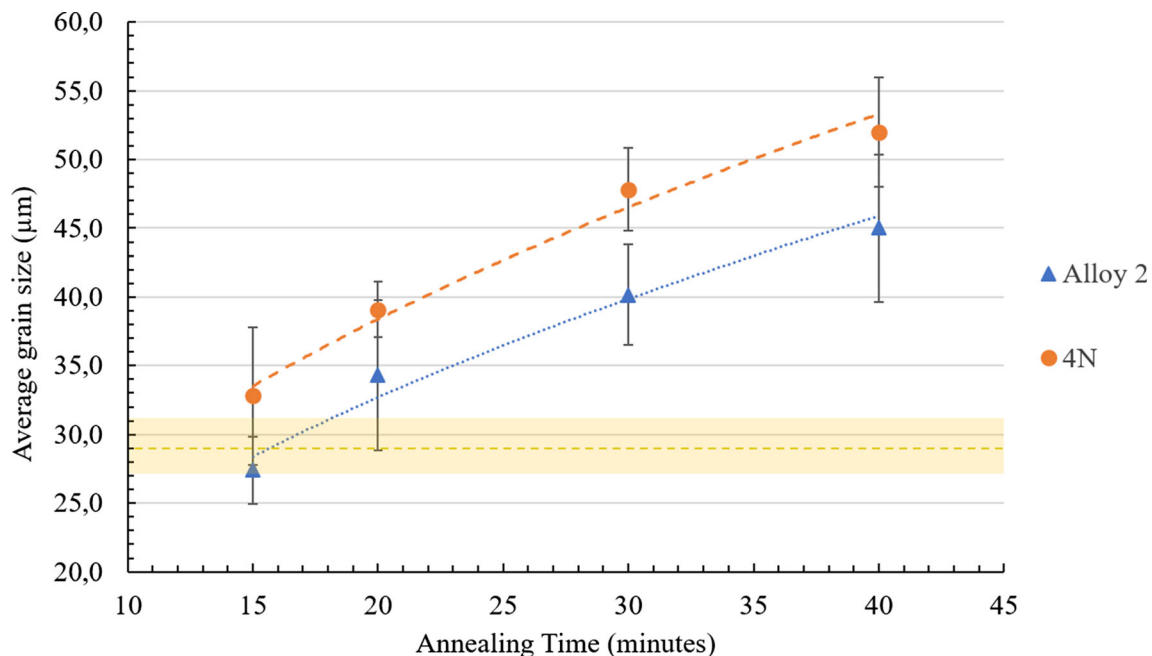|	Annealing time	Hardness, HRB
Alloy 4N	15 min	110.7 ± 0.5
	20 min	110.2 ± 0.3
	30 min	110.0 ± 0.8
	40 min	111.1 ± 0.8
Alloy 2	15 min	111.1 ± 0.1
	20 min	111.7 ± 0.8
	30 min	111.5 ± 1.1
	40 min	110.4 ± 1.1

Figure 13 Grain size at different annealing times during first annealing of Alloy 4N (orange spot), Alloy 2 (Blu triangle). Yellow dashed line represents the grain dimension of the refined alloy after the first annealing, and the highlighted area shows the statistical error
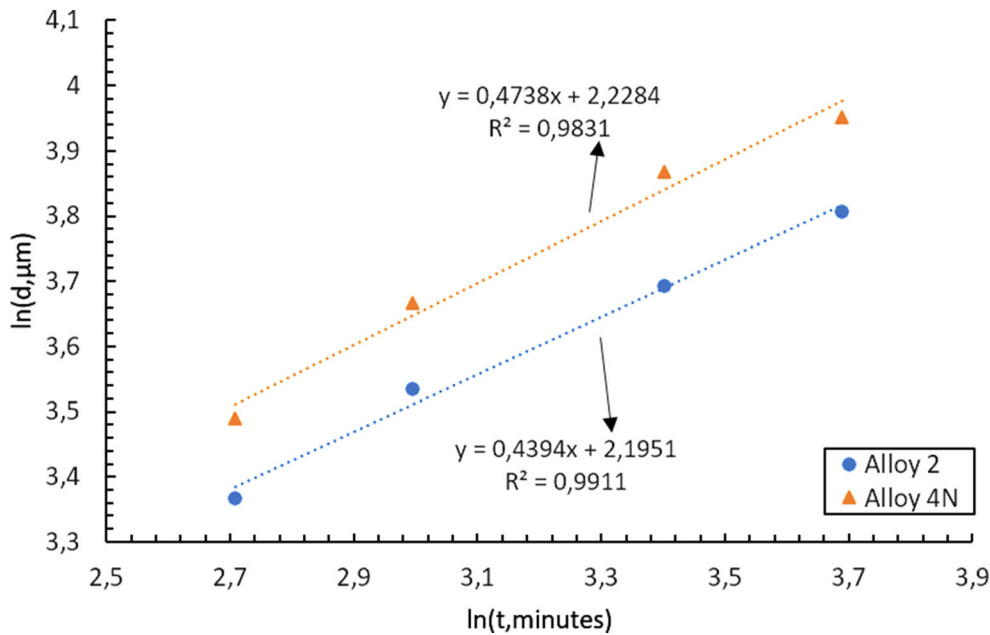
Figure 14 Linear fitting of grains dimension vs. annealing time of Alloy 2 and 4N with Eq.2

material and temperature and *n* is the grain growth exponent, this value in the analysis is equal to 2. In this case, d_o cannot be considered because, as in other studies (Ref 19), the initial recrystallized grains are very small in comparison with the final dimension. It is possible to use a simplified version of eq.1:

$$d = (Kt)^{1/n} \tag{Eq 2}$$

According to the Burke and Turnbull analysis, the n value of the pure metal is 2 (Ref 18). However, in most experimental studies on alloys, n values have been reported to be more than 2 due to the drag effects of the solute, which lower the grain boundary mobility. The constants n and K of equation (2), obtained from the graph in Figure 14, have the values 2.2 and 9.0 for 4N alloy and 2.2 and 9.3 for Alloy 2. "n" is greater than the ideal value of 2 due to the presence of numerous solute elements. There are not differences in terms of grain growth exponent from alloy 4N and 2. The two alloys differ in the K value, that is related to the activation energy of boundary diffusion. In particular, a decrease in the K value in alloy 2 can be observed probably due to the presence of zinc. Further grain growth rate analysis at different temperatures is required to evaluate the variation of activation energy as conduct in (Ref 18).

4. Conclusions

In this study, it was observed that iridium absence in 18 kt alloys leads to a considerable increase in the dimension of crystals in the cast products. However, it was also observed that the use of a more powerful cooling system leads to a reduction in the grain size after the casting process. It was also noted that the absence of refiner does not affect the hardness trend and therefore the work hardening during the whole process. A very small quantity of ordered phase AuCuI has been detected in XRD analysis in every step of the production process in all the examined alloys; this not seems to influence the hardening

behavior. In the first annealing, both the not refined alloys show a strong reduction in the crystalline dimension; besides, a remarkable inhomogeneity in the recrystallized grain size is recorded, probably caused by the high dimension of starting crystals domains. After the second annealing, alloy 2 and 4N show a more uniform microstructure with a size comparable to that obtained with the refiner.

Alloy 4N does not have a color commercially similar to the alloy 1 and it has the highest average grain size and the greatest degree of inhomogeneity after annealing. Instead, alloy 2, characterized by the absence of iridium as 4N, showed similar grain size, color, strain hardening behavior and corrosion resistance if compared to the iridium containing one (alloy 1). So, alloy 2 can be considered suitable for possible substitution of the alloy 1.

Furthermore, it was found that a reduction in the annealing time in the first annealing, while keeping the other process parameters unchanged, can reduce the grain size without compromising stress recovery in both not refined alloys. Alloy 2 shows a slightly better grain reduction respect to 4N, confirming the previously reported results. Burke and Turnbull's analysis seems to fit well the grain growth, and alloy 2 and 4N have a grain growth exponent n=2,2 and differ from each other by the K value, slightly higher in alloy 4N (probably due the presence of Zinc).

Concluding alloy 2 (iridium free) can replace the refined alloy (alloy 1) in the production of gold hollow chains, with a lower cost of raw material and less problem in surface finishing.

Funding

Open Access

References

1. C.W. Corti, Jewellery Alloys—Past, Present and Future, *Jewellery Mater. Congress*, (2019), p 1–24
2. M. Riabkina, L. Gal-Or, Y. Fishman and G. Iram, Grain-Refined Recrystallized 14-Carat Gold Alloy—Effect of Small Additions of Elements in an Au-Ag-Cu-Zn Alloy, *Gold Bull.*, 1984, **17**(2), p 62–69
3. Y. Ning, Properties and Applications of Some Gold Alloys Modified by Rare Earth Additions, *Gold Bull.*, 2005, **38**(1), p 3–8
4. J.P. Nielsen and J.J. Tuccillo, Grain Size in Cast Gold Alloys, *J. Dent. Res.*, 1966, **45**(3), p 964–969
5. D. Ott and C.J. Raub, Grain Size of Gold and Gold Alloys—A Review and Some Recent Developments, *Gold Bull.*, 1981, **14**(2), p 69–74
6. D. Ott, "Optimising Gold Alloys for Manufacturing - Ganoksin Jewelry Making Community," n.d., https://www.ganoksin.com/article/optimising-gold-alloys-for-manufacturing/
7. L. Pezzato, G. Magnabosco, K. Brunelli, M. Breda and M. Dabalà, Microstructure and Mechanical Properties of a 18Kt 5N Gold Alloy After Different Heat Treatments, *Metallogr. Microstruct. Anal.*, 2016, **5**(2), p 116–123
8. C. Cason, L. Pezzato, K. Brunelli, F. Furlan and M. Dabalà, Effect of the Composition and Production Process Parameters on the Microstructure, Residual Stresses, and Mechanical and Corrosion Properties of Gold Alloys Used in Industrial Jewelry Processes, *Gold Bull.*, 2017, **50**(3), p 259–266
9. D. Ott, Influence of Small Additions and Impurities on Gold and Jewelry Gold Alloys, *St. Fe Symp. Jewel. Manuf. Technol.*, 1997, p 173–196
10. X. Xiongzhi and B. Xiaojun, Grain Refinement of 18-Carat Au-Ag-Cu-Zn Alloy Containing Cerium, *Int. J. Met.*, 2016, **10**(1), p 100–105
11. F.J. Humphreys, M. Hatherly, Recrystallization and Related Annealing Phenomena," *Recrystallization and Related Annealing Phenomena*, 2nd ed. Elsevier, (1995)
12. M. Garcia-Gonzalez, S. Van Petegem, N. Baluc, M. Dupraz, V. Honkimaki, F. Lalire and H. Van Swygenhoven, Influence of Thermo-Mechanical History on the Ordering Kinetics in 18 Carat Au Alloys, *Acta Mater.*, 2020, **191**, p 186–197. https://doi.org/10.1016/j.actamat.2020.03.032
13. K. Yasuda and K. Hisatsune, Microstructure and Phase Transformations in Dental Gold Alloys—Determination of a Coherent Phase Diagram, *Gold Bull.*, 1993, **26**(2), p 50–66
14. R.M. German, M.M. Guzowski and D.C. Wright, The Colour of Gold-Silver-Copper Alloys - Quantitative Mapping of the Ternary Diagram, *Gold Bull.*, 1980, **13**(3), p 113–116
15. L. Miori and G. Rosa, The Colour-The Spectrophotometer like an Essential Tool to Guarantee Its Uniformity and Reproducibility in the Cosmetic Field, *Cosmet. Technol.*, 2015, **18**(2), p 36–40
16. C. Cason, L. Pezzato, M. Breda, F. Furlan and M. Dabalà, Effect of Microstructure and Residual Stresses, Generated from Different Annealing and Deformation Processes, on the Corrosion and Mechanical Properties of Gold Welding Alloy Wires, *Gold Bull.*, 2015, **48**(3–4), p 135–145
17. R. Süss, E. Van Der Lingen, L. Glaner and M. Du Toit, 18 Carat Yellow Gold Alloys With Increased Hardness, *Gold Bull.*, 2004, **37**(3–4), p 196–207
18. J.E. Burke and D. Turnbull, Recrystallization and Grain Growth, *Prog. Met. Phys.*, 1952, **3**(C)
19. Y.C. Huang, C.H. Su, S.K. Wu, and C. Lin, A Study on the Hall-Petch Relationship and Grain Growth Kinetics in FCC-Structured High/Medium Entropy Alloys, *Entropy*, 2019, **21**(3)